Passive Fuel Cell/Lithium-ion Capacitor Hybridization for Vehicular Applications

A. Macias[1,2,3]*, N. El Ghossein[5], J. Trovão[3,4], A. Sari[5], P. Venet[5], L. Boulon[1,2]

[1]Université du Québec à Trois-Rivières, Trois-Rivières, QC, G8Z 4M3, Canada

[2]Institut de Recherche sur l'Hydrogène, UQTR, Trois-Rivières, QC, G9A 5H7, Canada

[3]e-TESC Laboratory, Dept. Electrical & Computer Engineering, University of Sherbrooke, Sherbrooke, QC, J1K 2R1 Canada

[4]Canada Research Chair in Efficient Electric Vehicles with Hybridized Energy Storage Systems, University of Sherbrooke, Sherbrooke, QC, J1K 2R1 Canada

[5]Univ Lyon, Univ. Claude Bernard Lyon 1, Ecole Centrale de Lyon, INSA Lyon, CNRS, Ampère, 69130, France

Abstract

Electric recreational vehicles represent a new challenge in terms of power supply systems compared to the current light-duty electric vehicles, which achieve high performance and long-range. The recreational vehicles need to heed the limited dimension requirements while assuring the high requested power. This paper proposes an integration of Lithium-Ion Capacitor (LIC) with Fuel Cell (FC) without any power electronic device for a three-wheel electric motorcycle. Unlike other hybrid power supply systems, the proposed FC-LIC passive configuration is lighter, compact, more efficient, and simpler to implement. Due to the different impedance of the components the system is self-management, in which FC supplies the average power component and LIC operates as a low-pass filter. In this respect, a simulator is built based on experimental tests to study the system performance in terms of hydrogen consumption and FC degradation. Subsequently, the system is tested under three standard motorcycle driving cycles at three different FC system lifespan stages. The obtained results demonstrate that a passive topology can supply

the requested power along different FC stages of life and reported just an increment of 12% of hydrogen consumption at the oldest condition compared to the new condition.

Keywords: Electric motorcycle, Hybrid electric vehicle, Lithium-ion capacitor, Passive configuration, PEMFC, Recreational vehicle

Introduction

Electric vehicles are proposed to reduce greenhouse gas emissions from the transportation sector, mainly relying on non-renewable resources. Nowadays, electric vehicles can be powered by batteries or Fuel Cell (FC) systems. FC vehicles benefit from a higher driving range, zero-local emissions, and faster refueling than battery vehicles [1]. Even though FC vehicles are now available, their worldwide deployment is yet to come as they require more cost reduction and durability improvement. One of the FC systems durability vulnerabilities is their exposure to sudden power variations in vehicle applications, which leads to the deterioration of the internal electrolyte membrane [2]. In this respect, the high variations cause a decrement in the oxygen concentration of the FC and, consequently, a sudden power drop occurs [3]. The Fuel Cell Hybrid Electric Vehicles (FCHEV) couple a FC stack with an Energy Storage System (ESS) to cope with this issue. Through this, the vehicle can store regenerative energy, supplies high peaks of current, has higher range autonomy and obtains less capital and running cost [4]. Also, avoiding harsh changes in the FC current density is one of the low-cost water management method [5]. The coupling of the FC and the ESS to the DC bus is conducted in active and passive ways [6]. In the active topology, the components are connected to the DC bus via a DC-DC converter. The researchers prefer the active topology due to its high degree of freedom to control the power split between the sources. Through an Energy Management Strategy (EMS), the DC converter maintains a constant voltage level in the DC bus and splits the requested power among the components to enhance the performance and the lifespan of the system [7]. In this regard, it can be found in the literature that the multi-objective cost functions are able to reduce the hydrogen consumption while taking care of the FC stack and ESS [8, 9]. Contrary to the active configuration, the

passive one is a direct connection and self-management of the FC and the ESS to the DC bus, reducing the complexity, cost, and weight of the system [10]. In addition, the implementation of passive topology is simple and benefits from self-management due to the different impedance of the components.

The battery and the Supercapacitor (SC) have been broadly employed in the literature and industry as secondary ESS for vehicular applications [11]. The most common rechargeable battery used in vehicles is the lithium-ion battery because of its high energy density and high efficiency. However, its main disadvantages are the low power density, the reduced life cycle, and the long charging time. Regarding the SC, it is the most suitable device to provide rapid peaks of current due to the fast formation of the electric double layer at the interface between the electrodes and the electrolyte. Furthermore, the SC has higher specific power, a longer lifespan, and better resilience to different operation temperatures than the batteries. Nevertheless, SCs suffer from a low energy density and a high self-discharge, which can generate a high-power peak request if both systems do not have the same electric potential. In order to prevent this high inrush peak, a pre-charging strategy is needed, causing an increment in the startup time [12].

The Lithium-Ion Capacitor (LIC) is a novel hybrid device that may have a SC positive electrode (activated carbon), a battery kind negative electrode (carbon material pre-doped with lithium), and an electrolyte containing a lithium salt [13]. This composition yields good electrochemical properties with a relatively high-energy density and a high-power density, as illustrated in Fig. 1. Also, LIC operates in a voltage range of 2V and 3.8V, compared to SC cell that operates between 0V and its rated voltage (between 2.7V and 3V). Fig. 1 shows a comparison of the performance of the mentioned ESSs and FC, in which the specific energy (Wh/kg) is plotted versus the specific power (W/kg).
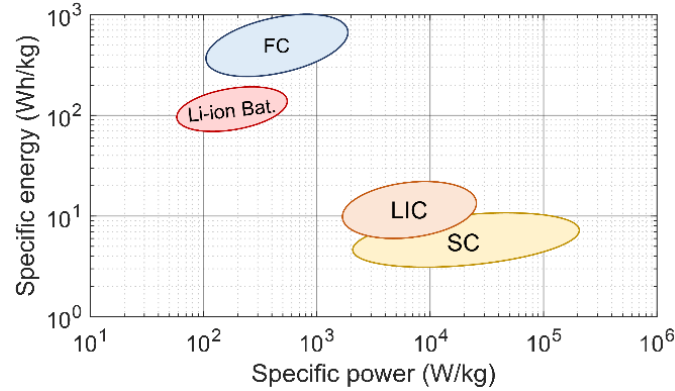
Fig. 1 - Ragone plot of FCs, Li-ion batteries, SCs and LICs.

Table 1 summarizes the main characteristics of three main ESS for electric vehicles [14, 15]. Owing to the mentioned characteristics, LICs are suitable for regenerative braking systems, high-requested power with deep discharging demand, and high cyclability applications. In this respect, it can be found in the literature that some of the works integrate the LIC into battery-based electric vehicles [16, 17].

Table 1 - Comparison of ESSs

Characteristics	Lithium-ion capacitor	Supercapacitor	Lithium-ion battery
Energy density	Low to medium	Low	High
Power density	High	Very high	Low
Charging time	In terms of tens of second or minutes	In terms of seconds or tens of second	In terms of hours or tens of minutes
Internal resistance	Low	Very low	High
Self-discharge	Medium	High	Low
Lifetime (cycles)	Long (~ 100,000)	Long (~ 1,000,000)	Relatively short (~ 5,000)

Based on the reviewed papers, some efforts have already been made concerning different ESSs with active and passive topologies for vehicular applications. However, so far, the hybrid systems with a secondary ESS are heavier, complex, and limited to provide either high peak currents or high autonomy. To the best knowledge of the authors, no efforts have been made to integrate a LIC into an electric recreational vehicle with a passive hybrid architecture. This type of vehicle is usually exposed to high requested power peaks and is limited in physical dimensions. In this respect, the selected passive configuration will reduce the weight and the volume of the system, enhance the FC system performance, and induce the absorption of the intermittent power fluctuations by the LIC. Moreover, the performance of

the hybrid system is analyzed in the MATLAB/Simulink environment at different stages of the life of the FC system under three motorcycle driving cycles. The rest of this paper is organized as follows. The vehicle modeling is detailed in Section 2. Section 3 presents the case study conditions and the utilized evaluation metrics. In Section 4, the performance analysis at different stages of the FC life is performed and discussed. Finally, the conclusion is given in Section 5.

Vehicle modeling

The principal objective of the manuscript is to analyze the performance of the new proposed FC-LIC hybrid system, shown in Fig. 2a, to power up a three-wheel electric vehicle (e-TESC-3W platform). The motorcycle studied in this manuscript, shown in Fig. 2b, is a recreational electric motorcycle utilized as an experimental test bench in e-TESC laboratory at the University of Sherbrooke [18].
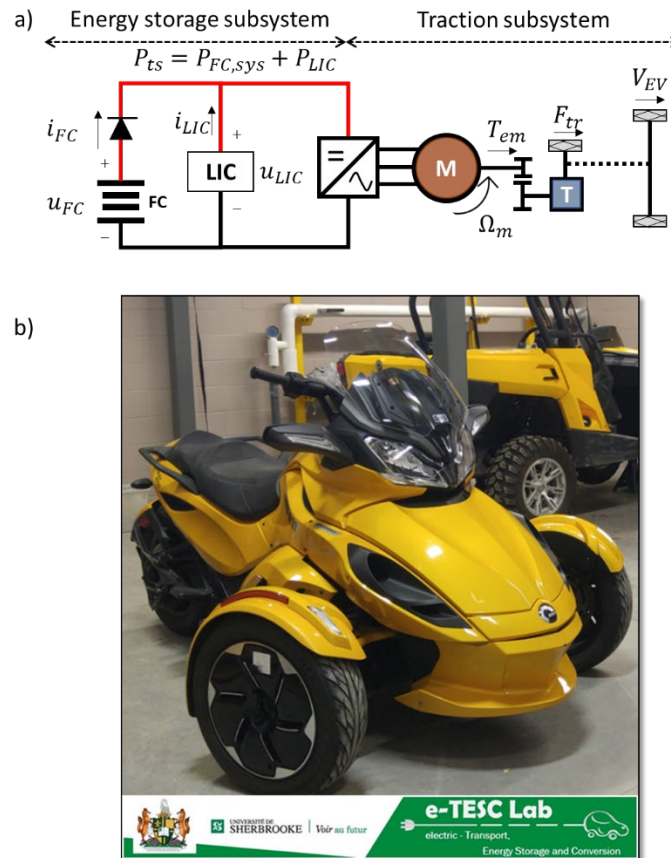

Fig. 2 - e-TESC 3W electric vehicle platform, a) architecture powertrain, b) picture.

Table 2 presents the main characteristics of this vehicle [19]. The e-TESC-3W platform powertrain has a permanent magnet synchronous machine (28kW and 96V) directly connected to the rear wheel. More details of the vehicle model are explained in [18]. The developed study in this article focuses on the performance of the FC-LIC power supply system at different stages of the life of the system.

Table 2 - Vehicle specifications

Variable	Symbol	Value	Units
Vehicle mass (w/o power source)	m_{eq}	350	kg
Typical rolling resistance coefficient	μ_{fr}	0.02	-
Typical aerodynamic drag coefficient	C_d	0.75	-
Vehicle front area	A_{aero}	1.25	m^2
Wheel radius	r	0.305	m
Belt transmission drive ratio	G_{gb}	5.033 (30:151)	-
Belt transmission drive efficiency	η_{gb}	95	%
Maximum vehicle speed	$V_{EV,max}$	140	km/h
Acceleration time (0 to 70 km/h)		8	s

Usually, recreational vehicles are characterized by their high acceleration behavior, lightweight, and compactness. Following the mentioned requirements, the component size that supplies the demanded energy is first defined by considering the weight and the volume of the system. Based on the electric machine specifications, a 27.3kW (135 cells) air-breathing FC is selected to supply the maximum stable power for a long time, imposed by the high-speed driving condition. The LICs operate as a low-pass filter, absorbing all the high-frequency components. Due to the direct coupling of the LIC bank and FC stack to the DC bus, they will share the same voltage value. To avoid any reverse current inside the FC, a diode is placed in series, as shown in Fig.2a. Consequently, the current splitting depends on the natural behavior of each component, and is defined as follows:

$$i_{FC} = \frac{(u_{FC}-u_{LIC})}{R_D} \tag{1}$$

where R_D is the dynamic diode resistance (with diode threshold voltage neglected), and the requested current is equal to the sum of FC and LIC currents. Therefore, the FC system can be turned-off, when the LIC voltage becomes higher than the Open Circuit Voltage (OCV) of the FC. In this regard, the studied

system uses 36 LICs, ULTIMO prismatic cells developed by JM Energy and JSR Micro, connected in series to assure a higher voltage at different system stages of life. Moreover, the DC bus voltage needs to be within a range of 80V – 120V that corresponds to the input voltage of the electric motor drive. As shown in Fig. 3, the LIC bank operational voltage is within the motor drive range, and most of the FC power under the three stages of life fall in the same range. Due to the parallel connection of the FC system and LIC bank they will share the same voltage, that means a high FC power will result in a low SOC_{LIC}. It is expected that the system will operate in a range of 20% - 70% of the SOC_{LIC}.
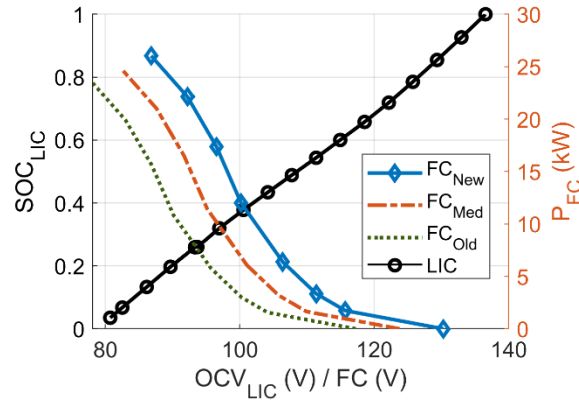

Fig. 3 - Correlation of LIC voltage with SOC and FC voltage with output power.

In addition, only one branch of LIC is selected in order to minimize the dimensions of the system. The LIC pack has a total energy of 157Wh, which is enough to buffer the high dynamics. For comparison purpose, to reach the same storage of energy capacity, the mass of a SC bank is almost the double. Also, the selected LIC banks operates as a low-pass filter with a cut-off frequency of 69mHz based on the capacitance of 91.6F and the equivalent series resistance of $25.2m\Omega$ of the LIC pack.

Traction subsystem

The traction subsystem part of the vehicle model is assumed as a static model of the electric machine and its drive, and Newton's second law is used to explain the motion interaction with the road. It is considered

that an internal control loop regulates the motor torque to achieve the desired speed, considering the motor efficiency map [18]. The fundamental vehicle model equations are represented as follows:

$$\frac{dV_{EV}}{dt} = \frac{(F_{tr} - F_{env})}{m_{eq}} \tag{2}$$

$$F_{tr} = (G_{gb}/r)T_{em}\eta_{gb}^{\beta} \tag{3}$$

$$F_{env} = F_{roll} + F_{grade} + F_{air} \tag{4}$$

$$F_{roll} = m_{eq}g\mu_{fr}\cos\theta \tag{5}$$

$$F_{air} = 0.5\rho_{air}A_{aero}C_dV_{EV}^{2} \tag{6}$$

$$F_{grade} = m_{eq}g\sin\theta \tag{7}$$

$$\Omega_m = (G_{gb}/r)V_{EV} \tag{8}$$

where F_{tr} is the traction force (N), F_{env} is the vehicle traction force resistance (N), m_{eq} is the vehicle mass (kg), G_{gb} is the gearbox transmission ratio, r is the wheel radius (m), T_{em} is the electric machine torque (N m), η_{gb} is the gearbox transmission efficiency, β is a discrete value that takes the value of -1 when the vehicle is in the braking mode and the value of 1 otherwise, g represents the gravity constant and θ is the slope of the road. The studied vehicle integrates a hybrid braking system in the rear wheel to recover a portion of the braking force into an electric energy. This system can recover an average of 10% from the total braking force that is distributed between the front and rear wheels, and a maximum recovered power of 10kW. Considering that the reference torque is achieved with a drive efficiency (η_m) that considers the inverter and motor efficiency, the required power in watts into the machine to reach the desired speed, Ω_m (rad/s), is then calculated by:

$$P_{ts} = T_{em}\Omega_m\eta_m^{\beta} \tag{9}$$

The mathematical model of the vehicle was validated with an on-road driving test carried out in the e-TESC laboratory [18]. A comparison of the recorded data by the precision eDAQ acquisition system and the model estimation are shown in Fig. 4. The acquisition system is directly connected to the CAN bus and battery-management system and record the data with a frequency rate of 10 Hz. The Root Mean Square Error (RMSE) of the estimated speed is 0.42 and 1.7 for the simulated traction system power. The error value in the simulated traction power is due to the fast variations on the speed profile, resulting in rapid dynamic changes in the traction system power. This difference is also attributed to the simplified model used in the motor drive module and the used typical rolling and drag coefficients. However, for the performance assessment purpose of this paper by comparison, this model is considered adequate.
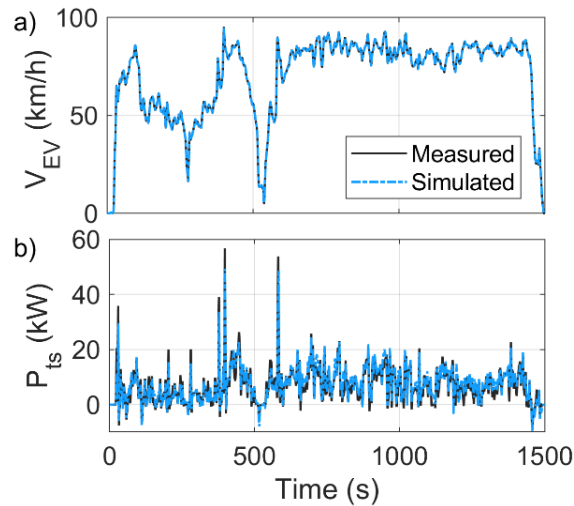
Fig. 4 - Experimental and simulation results for the three-wheel EV prototype, a) vehicle speed V_{EV} and b) requested machine power P_{ts}.

Fuel cell system

The FC system is a multiphysics element in which the voltage is influenced by external and internal factors such as current, temperature, hydrogen, and oxygen pressure. In the literature, the FC models are divided based on their physical insight and granularity in: mechanistic, black box, and semi-empirical [20]. The mechanistic models, which rely on thermodynamics, electrochemistry, and fluid mechanics differential

equations, have a high computational cost. On the other hand, the black box models are straight forward but they require a big dataset to reduce the uncertainties under new operating conditions. The semi-empirical models reach an acceptable compromise between complexity and accuracy by using experimental data and electrochemical based equations. Based on the mentioned characteristics, it has been opted, in this study to use an electrochemical based Proton Exchange Membrane Fuel Cell (PEMFC) model proposed by Amphlett et al [21]. This model considers the reversible potential E_{Nernst} (V), which is the maximum FC voltage, and the irreversible voltage losses which are: activation u_{act} (V), ohmic u_{ohmic} (V), and concentration u_{con} (V). It is assumed that all the cells (N_{FC}) in the stack have the same behavior. The PEMFC voltage u_{FC} (V) is calculated by:

$$u_{FC} = N_{FC}(E_{Nernst} + u_{act} + u_{ohmic} + u_{con}) \tag{10}$$

$$E_{Nernst} = 1.229 - 0.85 \times 10^{-3}(T_{FC} - 298.15) + 4.3085 \times 10^{-5}T_{FC}[\ln(p_{H2}) + 0.5\ln(p_{O2})] \tag{11}$$

$$\begin{cases} u_{act} = \xi_1 + \xi_2 T_{FC} + \xi_3 T_{FC} \ln(CO_2) + \xi_4 T_{FC} \ln(i_{FC}) \\ C_{O_2}^* = \dfrac{p_{O2}}{5.08 \times 10^6 \exp(-498/T_{FC})} \end{cases} \tag{12}$$

$$u_{ohmic} = -i_{FC} R_{internal} = -i_{FC}(\zeta_1 + \zeta_2 T_{FC} + \zeta_3 i_{FC}) \tag{13}$$

$$u_{con} = \alpha \ln(1 - i_{FC}/i_{FC,max}) \tag{14}$$

where the temperature of the stack T_{FC} is assumed to be uniform (K), p_{H2} is the hydrogen partial input pressure (Pa), p_{O2} is the oxygen partial input pressure (Pa), ξ_n (n = 1, …, 4) are empirical coefficients, $C_{O_2}^*$ is the oxygen concentration (mol/cm^3), i_{FC} is the FC operating current (A), $R_{internal}$ is the internal resistor (Ω) defined by the three empirical coefficients ζ_n (n = 1, …, 3), α is a semi-empirical parameter related to the diffusion mechanism (0.3$\leq \alpha \leq$1.8), and $i_{FC,max}$ is the maximum current (A). As this FC model is air-breathing, the oxygen partial pressure is approximated to 21% of the cathode pressure, which is the oxygen content of the air. Regarding the hydrogen partial pressure, it is approached to 99% of the anode pressure.

The cathode pressure is computed by an empirical equation in terms of FC current, on which the airflow mainly depends. The current flow, is then calculated by:

$$p_{ca} = a_1 + a_2 i_{FC} + a_3 i_{FC}{}^2 + a_4 i_{FC}{}^3 \qquad (15)$$

Where the anode inlet pressure p_{an} has been maintained at 0.2 bar above the cathode pressure p_{ca} [22]. This is to reduce the nitrogen crossover, enhance the cell stability, and purge the formed water through the cathode.

The empirical parameters of the electrochemical model are extracted offline with a metaheuristic algorithm based on the experimental dataset reported in [22]. This kind of approach has been implemented in previous works, due to their robustness, flexibility, and capabilities to compute the linear and nonlinear parameters of a PEMFC model [23]. The tuned semi-empirical model performance is compared with the single cell dataset found in the FCvelocity-9SSL Ballard datasheet, as shown in Fig. 5, and reported a RMSE of 0.0052. The polarization curve is chosen because it is one of the most common methods of testing a FC, which displays the voltage output for a given current load.
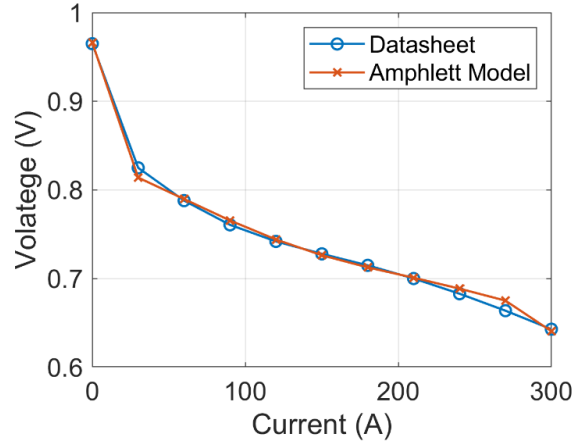

Fig. 5 - Comparison of the Amphlett model and the manufacturer polarization curve for a single cell.

The FC thermal behavior is modeled by the conservation of energy law, which is comprehensively explained in [24]. The energy balance of the FC system temperature dynamic is calculated by:

$$\frac{dT_{FC}}{dt} = \frac{Q_{heat} - Q_{conv}}{MC_{FC}} \tag{16}$$

$$Q_{heat} = N_{FC}i_{FC}(1.254 - u_{FC}) \tag{17}$$

$$Q_{conv} = H_{FC}(T_{FC} - T_{amb}) \tag{18}$$

where the change in the FC temperature T_{FC} (K) is generated by Q_{heat} the difference of heat in the FC (W) and Q_{conv} the heat dissipated due to convection (W). The thermal capacity of the FC MC_{FC} (J/K) and heat transfer coefficient H_{FC} (W/K) are in-depth discussed in [24].

The total FC system power $P_{FC,sys}$ (W) is obtained by subtracting the losses from the hydrogen electrochemical reaction, as shown in Eq. (13). The losses consist of fan power P_{fan} (W), which is considered as constant (200 W), and the power of the compressor P_{comp} (W).

$$P_{FC,sys} = P_{FC} - P_{comp} - P_{fan} \tag{19}$$

Based on the datasheet of the FC, the hydrogen consumption W_{H_2} (Standard Liter Per Minute), is approximated by a linear function in terms of the number of cells and the current [25].

$$W_{H_2}(t) = 0.00696i_{FC}N_{FC} \tag{20}$$

The efficiency of the FC system is calculated considering the consumed energy by the liquid and air-cooling auxiliaries systems.

$$\eta_{FC,sys} = P_{FC,sys}/\left(W_{H_2} \times HHV\right) \tag{21}$$

where HHV represents the hydrogen high heating value.

Lithium-ion capacitor

A LIC is a hybrid ESS that combines the energy storage mechanisms of lithium-ion batteries and SC. This hybrid system is usually composed of a lithium-ion battery negative electrode and a SC positive electrode [14]. It can supply a relatively high energy value and high peaks of power over long cycle a life. These

advantages make it suitable for hybrid electric vehicles to support the primary power supply system under high-dynamic and fast-transmit load current profiles [26]. The electrochemical process inside the LIC cell occurs within a voltage range of 2.2 to 3.8 V. The neutral state is considered at 3V when no ions are absorbed at the positive electrode. In the charging process from 3V to 3.8V, the electrolyte salt breaks down, the Li^+ cations are intercalated in the carbon material anode, and the negative ions are adsorbed at the surface of the activated carbon electrode. The discharge from 3V to 2.2V generates an exchange of ions between both electrodes. The positive Li^+ ions are deintercalated from the negative electrode and adsorbed at the surface of the positive one [27].

It was previously proved that LIC technology can operate in a wide range of temperatures (-10 °C to 60 °C), and its electric characteristics; capacity and equivalent resistance, presents minimal changes when it operates in a range of 25 °C to 50 °C [28]. From this perspective, it is assumed that the selected LIC will operate within this temperature range and their electric properties will remain constant. Following this assumption, LIC is represented by a classical equivalent circuit model in this paper, and no thermal model is included. The classical RC model includes a capacitance element and an equivalent series resistance (ESR), as shown in Fig. 6 [29]. The self-discharge, represented as a parallel resistance with the capacitor, is omitted in this work due to the low impact in the short-term and constant operation. This self-discharge rate varies depending on the SOC level, and is approximated to be less than 1% per day [30].
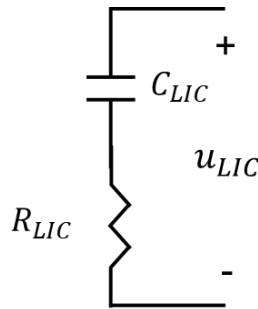

Fig. 6 - LIC equivalent circuit model.

During charge of the LIC, the electrical behavior is calculated as follow:

$$u_{LIC}(t) = R_{LIC} * i_{LIC}(t) + \int \frac{i_{LIC}(t)dt}{C_{LIC}} + u_C(t-1) \tag{22}$$

where at the initial state $u_c(t_0)$ is equal to the OCV of the LIC (V), i_{LIC} is the current across the LIC (A), C_{LIC} is the equivalent capacitance value of the LIC (F) and R_{LIC} is the ESR of the LIC (Ω). The equivalent constant parameters, $R_{LIC} = 1m\Omega$ and $C_{LIC} = 3300F$, are obtained from the JM Energy manufacturer datasheet. The main electric parameters of the selected LIC are presented in Table 3.

Table 3 - 3300F ULTIMO LIC specifications

Variable	Value	Units
Voltage range	2.2 – 3.8	V
Max. charging current	125	A
Max discharging current	360	A
Nominal capacitance	3300	F
Energy density	13	Wh/kg
Power density	10	kW/kg

The performance of the RC model has been tested on the presented test bench in Fig. 7a. A square current signal, which charges completely the LIC up to 3.8V with a current of 100A and then discharge it completely until 2.2V with a current of -100A, was imposed as shown in Fig. 7b. The mentioned test was carried out in a climatic chamber at 40 °C in the AMPERE Laboratory of Lyon 1 University. The estimated output voltage of the RC model is compared with the real LIC voltage in Fig. 7b, in which the estimation reported a RMSE of 0.04. For the sake of this paper the estimation of the utilized RC model reaches an acceptable voltage approximation.
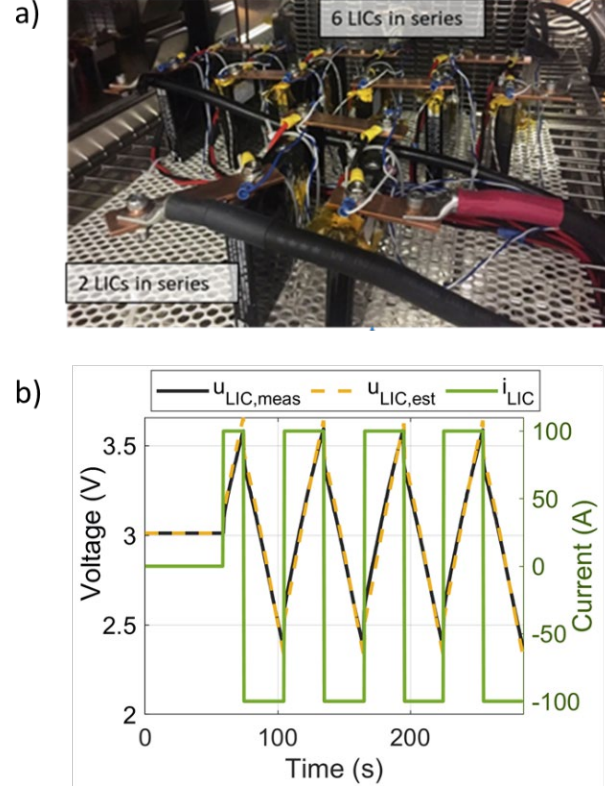
Fig. 7 - LIC test bench setup in a climatic chamber, and voltage comparison during continuous cycling of the LIC prismatic cells.

The coulomb counting method is used to calculate the LIC state of charge (SOC) due to its low computational effort and easy implementation in the simulation.

$$SOC_{LIC}(t) = SOC_{LIC}(t_0) + \frac{1}{3600C} \int i_{LIC} \, dt \tag{23}$$

where $SOC_{LIC}(t_0)$ represents the initial value of state of charge, and C is the LIC's ideal capacity (Ah). In [31], a LIC has been characterized at different ambient temperature conditions from -20 °C to 60 °C. It is observed that at 25 °C, the relationship between SOC and OCV can be represented as a linear function. Based on experimental data, a first-order function is fitted, as shown in Fig. 8, resulting in the next equation:

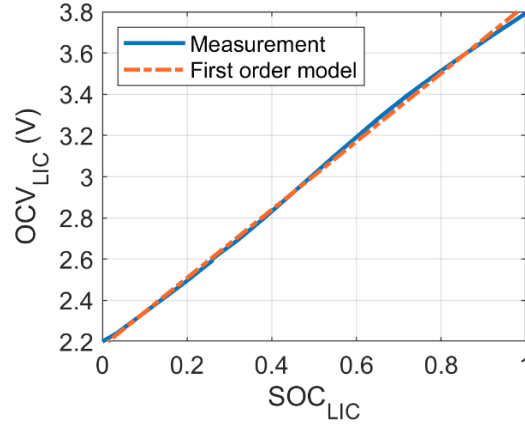$$OCV_{LIC}(t) = [1.655 * SOC_{LIC}(t)] + 2.178 \tag{24}$$

Fig. 8 - OCV-SOC correlation.

Case study

Standard driving cycles ease the evaluation of the performance and lifecycle costs of emerging vehicular technologies. They avoid bias in the performance results compared to on-drive conditions, because they represent a more distributed and richer signal built from a collection of daily and real motorcycle driving behavior from different countries. In this respect, some of the driving cycles used for the certification of motorcycles, which are all chassis-dynamometer type, are the NEDC profile by the European Union, the Class III FTP-72 profile by the United States Environmental Protection Agency (US EPA), and the Worldwide Motorcycle Test Cycle (WMTC) Class3-1 that represents an on-road worldwide vehicle operation [32]. Table 4 summarizes the main characteristics of the selected driving cycles.

Table 4 - Motorcycle driving cycle characteristics

Variable	NEDC	FTP-72	WMTC
Relative positive acceleration	$0.11 m/s^2$	$0.16 m/s^2$	$0.14 m/s^2$
Cycle Average Driving Speed	32.4km/h	30.6km/h	53.1km/h
Maximum speed	117 km/h	88.7km/h	108.1km/h
Duration	1178s	1369s	1820s
Distance	10.62km	11.65km	26.84km

Although the component size is the same in all the driving conditions, the hybridization ratio (HR) is calculated to give a clearer idea of the contribution of the LIC into the delivered power. The HR is defined

as the percentage of the maximum power component of the LIC ($P_{LIC,max}$) to the maximum requested power of the traction submodule ($P_{ts,max}$).

$$HR = \frac{P_{LIC,max}}{P_{ts,max}} \tag{25}$$

System durability analysis

Most of the existing papers have merely focused on fuel consumption minimization. However, FC cost and durability are critical obstacles to speed up the FCHEV commercialization [33]. In this respect, the degradation rate is a complementary metric to evaluate vehicle performance with the proposed passive configuration. Based on the US Department of Energy (DOE) objectives for vehicle application, the End of Life (EOL) of a FC is defined as a 10% drop in the maximum power, and it should be reached after 5000 hours and 5000 startup/shutdown cycles. It was validated that the commercial FCs are capable of operating for 5000 hours with stable current steps, but they can just perform 1300 start/stop cycles [34]. In this context, start/stop cycling and load changing conditions are responsible for more than 80% of the FC degradation. Table 5 summarizes the degradation conditions and their corresponding FC performance losses [35].

Table 5 - Coefficients of FC performance degradation.

Variable	Coefficient
k_1	0.00126 (%/h)
k_2	0.00196 (%/cycle)
k_3	5.93×10^{-5} (%/cycle)
k_4	0.00147 (%/h)
k_5	0.002 (%/h)

The percentage of FC degradation, Δ_{FC}, is calculated as the sum of FC degradation under each condition.

$$\Delta_{FC} = k_1 t_1 + k_2 n_1 + k_3 n_2 + k_4 t_3 + k_5 t_{FC_{ON}} \tag{26}$$

where k_1 is the low power coefficient (less than 5% of maximum power), k_2 represents one start-stop coefficient, k_3 is the fast-dynamics coefficient (absolute value of power variations more significant than 10% of maximum power per second), k_4 is the high power coefficient (more than 90% of maximum power), k_5 is the natural decay rate (the time that FC is under operation), n_j (j = 1,2) is the number of cycles, t_i ($i = 1,2, FC_{ON}$) is the operational time in its corresponding condition. The State of Health (SOH) indicator tracks the performance evolution of the FC, due to degradation, by comparing it with the beginning of life state [36]. This degradation represents the loss of power that the FC can provide for a specific current value. Consequently, to provide the same power level with a lower SOH, the system output current needs to increase. The SOH is calculated as follows:

$$SOH_{FC} = SOH_{FC,init} - \frac{\Delta_{FC}}{\Delta_{FC,max}} \tag{27}$$

where $SOH_{FC,init}$ is the initial SOH that corresponds to the new condition (100%), and $\Delta_{FC,max}$ represents the maximum percentage of FC degradation defined by the DOE (10%).

Concerning the LIC degradation, it was proved that the LICs are a long-life energy storage system. In [13], calendar aging of the cells was assessed. When the cells were stored at a SOC of 50%, a negligible decrease of the capacitance was noticed after 20 months of aging. Moreover, when the cells were continuously cycled over the complete potential window, they were far from reaching the EOL criterion even after 450000 cycles. These results were confirm in a second study, where a LIC has been cycled continuously with a dynamic power profile at a variable temperature for more than two years and reported just a 4% capacity loss [37]. As a result, it can be assumed that the degradation of the LIC is negligible in comparison with the FC one.

Results analysis

The vehicle performance using the proposed passive hybrid system is evaluated under three driving cycles considering the degradation of the FC system. This study is carried out with the e-TESC-3W platform,

explained in section 2. As discussed in Section 3, the LIC suffers from a small percentage of degradation compared to the FC system. In this respect, each driving cycle is implemented into an arrangement at three different stages of the FC life, namely New (SOH 100%), Med (SOH 50%) and Old (SOH 0%).

Fig. 9a shows the speed profile of the NEDC driving cycle. In this profile, the vehicle operates for almost 1000s with a speed level of less than 50 km/h, and it has several full-stop conditions. These characteristics make the FC works at low current region, as shown in Fig. 9b. Due to the series diode connected to the FC, the requested power is supplied only by the LIC bank at the beginning until its voltage level reaches the same value as the FC OCV. However, the OCV level decreases depending on the stage of health, and this makes the newer FC work sooner than the older ones, as seen in Fig. 9b. As shown in the zoom on Fig. 9b, the older FCs operate in higher currents to deliver the same requested power from the powertrain. In Fig.9c, the LIC SOC fluctuates around different values depending on the FC SOH. Moreover, the LIC bank operates for a longer period in low power when the FC system is newer, as observed in the Fig. 9d. Also, from Fig. 9a and Fig. 9d, it can be deduced that the hybridization ratio is about 12%.
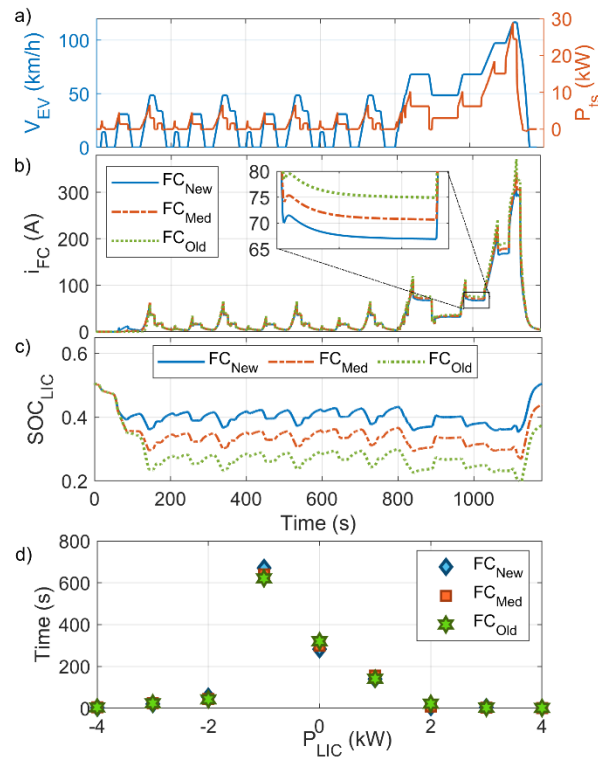

Fig. 9 - NEDC results from the Simulink model.

Table 5 summarizes the performance metrics for the complete driving cycle. The system presents a lower hydrogen consumption in newer FCs due to their smaller current operation. However, the variation in the Δ_{FC} values are very small because most of the degradation comes from the initial startup event and natural decay, which are the same for all the cases. As it is observed in Fig. 9c, the three cases have different final SOCs. The last column of Table 6 (ΔSOC_{LIC}) represents the difference between the final and initial LIC SOC. A negative ΔSOC_{LIC} implies that the LIC finishes with less energy than the initial one.

Table 6 - Breakdown analysis for NEDC profile

FC	SOH_{FC}	W_{H_2} (gr)	Δ_{FC} (%)	ΔSOC_{LIC} (%)
FC_{New}	100%	58.8	0.0060	-0.1
FC_{Med}	50%	56.6	0.0062	-6.6
FC_{Old}	0%	59.6	0.0067	-13.2

The same analysis has been followed for all the driving cycles. The second driving cycle, FTP-72, presents a high relative positive acceleration due to the consecutive high-power demand accelerations. However, it has a low average speed that makes the FC and LIC operate in low currents, as shown in Fig.9b. It is observed that although the SOC_{LIC} drop up to a 20%, the corresponding u_{LIC} is always within the operating motor driver voltage. As shown in Fig. 10d, the LIC will operate most of the time in negative power. That means the LIC is absorbing the surplus power while the FC power is adjusted. Although the average and maximum requested power from this profile are lower compared to the previous NEDC cycle, the HR is about 30%. This results from the higher acceleration rate that requires the LIC to contribute more to the requested power peaks.
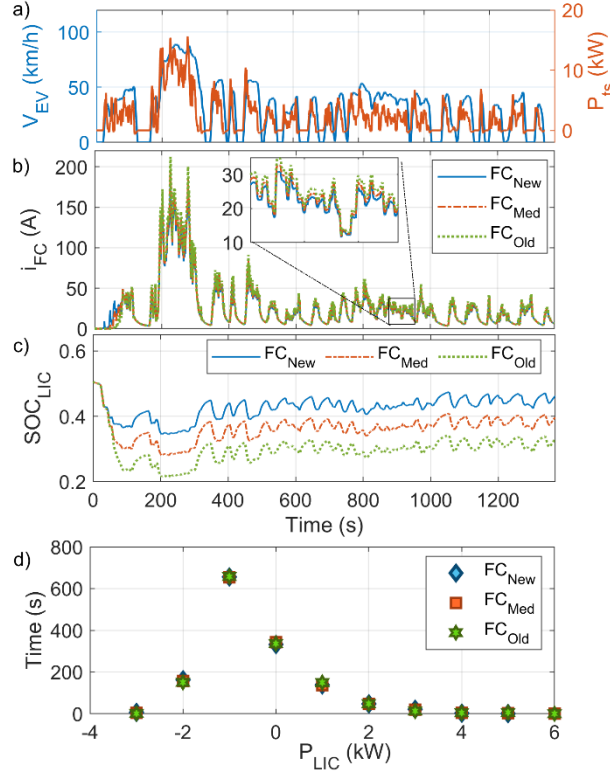
Fig. 10 - FTP-72 results from the Simulink model.

The system performance and FC degradation are summarized in Table 7. It is observed that there is a higher fuel usage in the older FC system because the old system operates at higher current values. On average, the increment of Δ_{FC} is consistent with the high relative positive acceleration of this profile. Moreover, by the time the FC gets degraded, it increases the load changes and reduces the low-power phases of the FC current trend. The FC degradation caused by load changing has a much more significant effect than low-power, as explained in [38], occasioning an increment in Δ_{FC} with older FC systems.

Table 7 - Breakdown analysis for FTP-72 profile

FC	SOH_{FC}	W_{H_2} (gr)	Δ_{FC} (%)	ΔSOC_{LIC} (%)
FC_{New}	100%	46.5	0.0057	-4.4
FC_{Med}	50%	48.6	0.0071	-11
FC_{Old}	0%	51.1	0.0088	-17.3

The WMTC driving cycle, shown in Fig. 11, has the highest average speed and duration. It is composed of 3 parts. The first part consists of eight micro-trips, the second part represents secondary rural roads, and the third part is a micro-trip on a highway. In the last part of the profile, as shown in Fig. 11b, it is more evident that the new FC operates at lower currents compared to the degraded FC systems. As observed in Fig. 11c, the last seconds of the driving cycle presents a low speed which allow the FC system to recharge the LIC and, in the new condition, to finish at the same initial SOC_{LIC}. From Fig. 11d, it can be noted that the LIC, as the FC, operate in higher power due to the higher average driving speed and result in a 34% of HR.
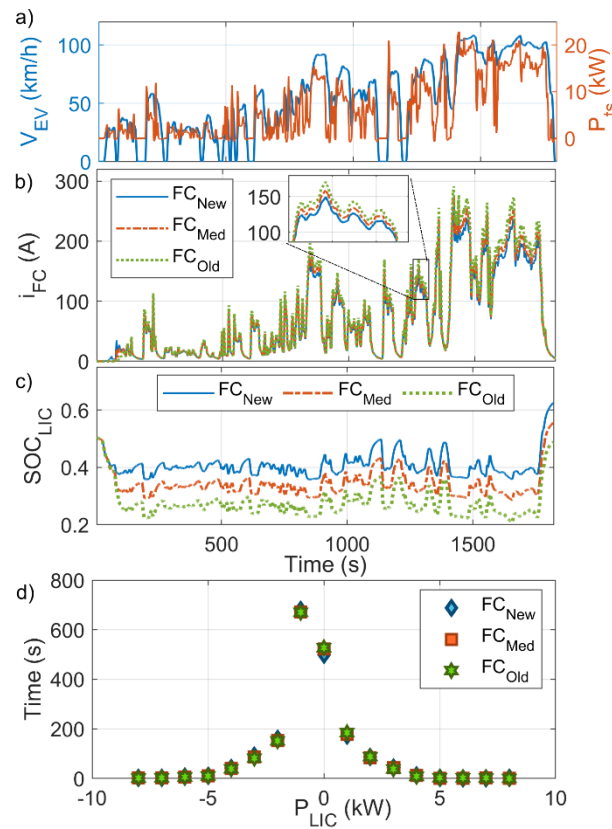

Fig. 11 - WMTC results from the Simulink model.

The summary of the performance analysis of the WMTC driving cycle is reported in Table 8. As expected, due to the long duration and high average speed of WMTC, the hydrogen consumption and FC degradation values are higher than the other driving cycles. The high current operation is mostly located in the third part of the driving cycle, which has an 84km/h and a top speed of 110km/h, and it has a long-time presence in the older systems.

Table 8 - Breakdown analysis for WMTC profile

FC	SOH_{FC}	W_{H_2} (gr)	Δ_{FC} (%)	ΔSOC_{LIC} (%)
FC_{New}	100%	164.7	0.0136	11.8
FC_{Med}	50%	174.5	0.0184	4.9
FC_{Old}	0%	185.8	0.0233	-1.7

In the three studied driving cycles, the FC-LIC passive hybrid system can supply the requested power and operate within the motor driver voltage range. However, the SOC_{LIC} reaches very low values in the FC_{Old} condition, that can lead to low performance of the LIC. Besides, it is difficult to compare the three life stages as there is no guarantee that they will finish in the same final SOC. In this sense, the driving profiles have been tested under different initial SOC_{LIC} levels; 0.2, 0.3, 0.4, 0.5, 0.6, 0.7 and 0.8. Fig. 12 gives a better point of comparison; it plots the hydrogen consumption for a given ΔSOC_{LIC}. The ΔSOC_{LIC} will vary depending on the performance of the FC system and the requested power behavior. It demonstrates that a system with an old FC will have a higher hydrogen consumption with any initial SOC_{LIC}. On average, compared to the FC_{New} condition, the increment in hydrogen consumption is by 12% for the FC_{Old} and 6% for the FC_{Med}. As shown in Fig. 12c, the highest hydrogen consumption in the WMTC driving cycle is in linked to the higher ΔSOC_{LIC} values.
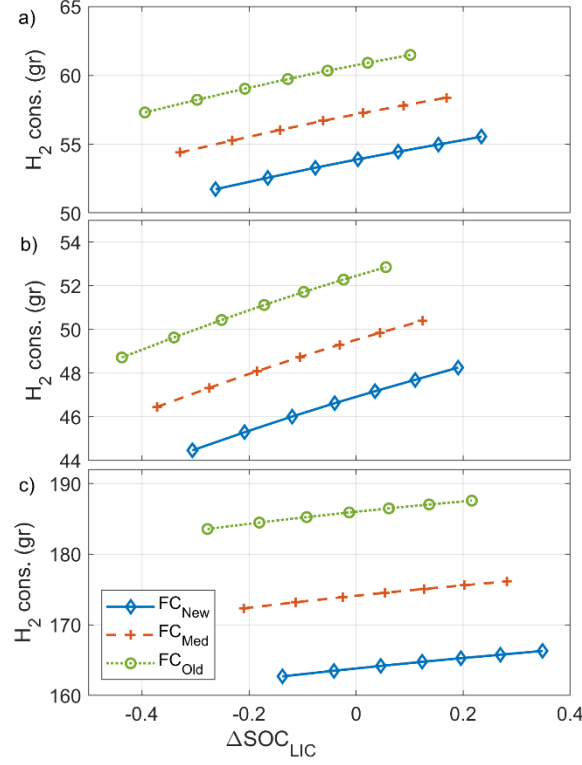
Fig. 12 - Hydrogen cons. versus ΔSOC_{LIC} for the driving cycles: a) NEDC, b) FTP-72, and c) WMTC.

Conclusions

This paper investigates vehicle performance using a new hybrid power supply system for automotive applications. The proposed system integrates a FC stack and a LIC bank in a passive configuration to furnish the requested power of a three-wheel electric motorcycle. In this respect, the power splitting is done without an energy management strategy due to the different impedance of the components connected in the DC bus. The performance assessment is done under three stages of the FC stack life, 100%, 50%, and 0% SOH. The results show that the system can supply the requested power, and the selected LIC size has enough energy to operate the DC bus between the desired voltage levels (80V - 120V). In addition, the reported HR has a direct link to the relative positive acceleration of the driving cycle. However, the SOC_{LIC} operates at lower values by the time that the FC gets degraded.

In terms of hydrogen consumption, on average, there is an increment of 12% for the FC_{Old} and 6% for the FC_{Med} compared to the FC_{New} condition. Regarding the FC degradation, an increment in Δ_{FC} is observed in the FTP-72 and WMTC driving cycles, which has a high relative positive acceleration and more stops along with the profile. Also, according to the reported information of both profiles, it appears that the Δ_{FC} of an old FC is almost two times more than the one at the beginning of life. Based on this, it can be concluded that in the more dynamic profiles, there will be an increment of Δ_{FC} while the FC deteriorates.

Future works can consider evaluating the passive configuration in more driving conditions, as the FC hybrid system is highly nonlinear, and its performance is heavily relying on the driving conditions. While this study shows the potential of a FC-LIC passive configuration, the implementation of this hybrid system on a real test bench should be practiced in upcoming studies. In this respect, first a small-scale test will be caried out to validate the proposed architecture and then the passive FC-LIC power supply system will be implemented in the e-TESC-3W platform. It should be noted that this implementation will be the first in its class, therefore different studies are needed to make sure about its safety and system integrity. Looking forward, one of the remaining challenges to reach more affordable FC vehicles is the component sizing that is directly related to the cooperation of the hybrid system components. Therefore, future works should focus on the integration of optimized sizing methodologies that consider the hydrogen consumption and power supply system degradation into the design phase. In addition, a sensitivity analysis of the component price is recommended due to their fluctuation that vary depending on the retail, acquisition volume, and technology readiness level.

Acknowledgments

Nomenclatures

Acronyms

DOE	US Department of Energy
EMS	Energy Management Strategy
EOL	End of Life
ESS	Energy Storage System
FC	Fuel Cell
FCHEV	Fuel Cell Hybrid Electric Vehicles
LIC	Lithium-Ion Capacitor
OCV	Open Circuit Voltage
RMSE	Root Mean Square Error
SC	Supercapacitor
SOH	State of Health
US EPA	United States Environmental Protection Agency
WMTC	Worldwide Motorcycle Test Cycle

References

[1]   Acar C, Dincer I. The potential role of hydrogen as a sustainable transportation fuel to combat global warming. International Journal of Hydrogen Energy 2018;45:3396-3406. https://doi.org/10.1016/j.ijhydene.2018.10.149.

[2]   Ao Y, Laghrouche S, Depernet D, Chen K. Lifetime prediction for proton exchange membrane fuel cell under real driving cycles based on platinum particle dissolve model. International Journal of Hydrogen Energy 2020;45:32388-401. https://doi.org/10.1016/j.ijhydene.2020.08.188.

[3]   Wang J. System integration, durability and reliability of fuel cells: Challenges and solutions. Applied Energy 2017;189:460-79. https://doi.org/10.1016/j.apenergy.2016.12.083.

[4]   Bendjedia B, Rizoug N, Boukhnifer M, Bouchafaa F, Benbouzid M. Influence of secondary source technologies and energy management strategies on Energy Storage System sizing for fuel cell electric vehicles. International Journal of Hydrogen Energy 2018;43:11614-28. https://doi.org/10.1016/j.ijhydene.2017.03.166.

[5]   Wang XR, Ma Y, Gao J, Li T, Jiang GZ, Sun ZY. Review on water management methods for proton exchange membrane fuel cells. International Journal of Hydrogen Energy 2020;46: 12206-29. https://doi.org/10.1016/j.ijhydene.2020.06.211.

[6]   Das HS, Tan CW, Yatim AHM. Fuel cell hybrid electric vehicles: A review on power conditioning units and topologies. Renewable and Sustainable Energy Reviews 2017;76:268-91. https://doi.org/10.1016/j.rser.2017.03.056.

[7]   Yue M, Jemei S, Gouriveau R, Zerhouni N. Review on health-conscious energy management strategies for fuel cell hybrid electric vehicles: Degradation models and strategies. International Journal of Hydrogen Energy 2019;44:6844-61. https://doi.org/10.1016/j.ijhydene.2019.01.190.

[8]   Hu X, Zou C, Tang X, Liu T, Hu L. Cost-optimal energy management of hybrid electric vehicles using fuel cell/battery health-aware predictive control. IEEE Transactions on Power Electronics 2019;35:382-92. https://doi.org/10.1109/TPEL.2019.2915675.

[9]   Wu X, Hu X, Yin X, Li L, Zeng Z, Pickert V. Convex programming energy management and components sizing of a plug-in fuel cell urban logistics vehicle. Journal of Power Sources 2019; 423:358-66. https://doi.org/10.1016/j.jpowsour.2019.03.044.

[10]   Arora D, Bonnet C, Mukherjee M, Raël S, Lapicque F. Direct hybridization of PEMFC and supercapacitors: Effect of excess hydrogen on a single cell fuel cell durability and its feasibility on fuel cell stack. Electrochimica Acta 2019;310:213-20. https://doi.org/10.1016/j.electacta.2019.04.073.

[11]   Lü X, Qu Y, Wang Y, Qin C, Liu G. A comprehensive review on hybrid power system for PEMFC-HEV: Issues and strategies. Energy Conversion and Management 2018;171:1273-91. https://doi.org/10.1016/j.enconman.2018.06.065.

[12]   Dépature C, Macías A, Jácome A, Boulon L, Solano J, Trovão JP. Fuel cell/supercapacitor passive configuration sizing approach for vehicular applications. International Journal of Hydrogen Energy 2020;45:26501-12. https://doi.org/10.1016/j.ijhydene.2020.05.040.

[13]   Ghossein NE, Sari A, Venet P. Effects of the Hybrid Composition of Commercial Lithium-Ion Capacitors on Their Floating Aging. IEEE Transactions on Power Electronics 2019;34:2292-99. https://doi.org/10.1109/TPEL.2018.2838678.

[14]   Lamb JJ, Burheim OS. Lithium-Ion Capacitors: A Review of Design and Active Materials. Energies 2021;14:979. https://doi.org/10.3390/en14040979.

[15]   Nadeem F, Hussain SMS, Tiwari PK, Goswami AK, Ustun TS. Comparative Review of Energy Storage Systems, Their Roles, and Impacts on Future Power Systems. IEEE Access 2019;7:4555-85. https://doi.org/10.1109/ACCESS.2018.2888497.

[16]   Soltani M, Ronsmans J, Kakihara S, Jaguemont J, Van den Bossche P, van Mierlo J, Noshim O. Hybrid Battery/Lithium-Ion Capacitor Energy Storage System for a Pure Electric Bus for an Urban Transportation Application. Applied Sciences 2018;8:1176. https://doi.org/10.3390/app8071176.

[17]   Goussian A, LeBel F-A, Trovão JP, Boulon L. Passive hybrid energy storage system based on lithium-ion capacitor for an electric motorcycle. Journal of Energy Storage 2019;25:100884. https://doi.org/10.1016/j.est.2019.100884.

[18]   Trovão JPF, Roux M, É M, Dubois MR. Energy- and Power-Split Management of Dual Energy Storage System for a Three-Wheel Electric Vehicle. IEEE Transactions on Vehicular Technology 2017;66:5540-50. https://doi.org/10.1109/TVT.2016.2636282.

[19]   Macías A, Kandidayeni M, Boulon L, Trovão J. Passive and Active Coupling Comparison of Fuel Cell and Supercapacitor for a Three-Wheel Electric Vehicle. Fuel Cells 2019;20:351-61. https://doi.org/10.1002/fuce.201900089.

[20]   Kandidayeni M, Macias A, Amamou AA, Boulon L, Kelouwani S, Chaoui H. Overview and benchmark analysis of fuel cell parameters estimation for energy management purposes. Journal of Power Sources 2018;380:92-104. https://doi.org/10.1016/j.jpowsour.2018.01.075.

[21]   Mann RF, Amphlett JC, Hooper MAI, Jensen HM, Peppley BA, Roberge PR. Development and application of a generalised steady-state electrochemical model for a PEM fuel cell. Journal of Power Sources 2000;86:173-80. https://doi.org/10.1016/S0378-7753(99)00484-X.

[22]   Zhao X, Li Y, Liu Z, Li Q, Chen W. Thermal management system modeling of a water-cooled proton exchange membrane fuel cell. International Journal of Hydrogen Energy 2015;40:3048-56. https://doi.org/10.1016/j.ijhydene.2014.12.026.

[23] Kandidayeni M, Macias A, Khalatbarisoltani A, Boulon L, Kelouwani S. Benchmark of proton exchange membrane fuel cell parameters extraction with metaheuristic optimization algorithms. Energy 2019;183:912-25. https://doi.org/10.1016/j.energy.2019.06.152.

[24] Oruganti PS, Ahmed Q, Jung D. Effects of Thermal and Auxiliary Dynamics on a Fuel Cell Based Range Extender. SAE Technical Paper 2018. https://doi.org/10.4271/2018-01-1311.

[25] Ballard Power Systems. FCvelocity-9SSL V4 Product Manual and Integration Guide, https://www.ballard.com/docs/default-source/spec-sheets/fcvelocity9ssl.pdf?sfvrsn=4aebc380_4; 2017 [accessed 14 June 2021].

[26] Zhang L, Wilkinson DP, Chen Z, Zhang J. Lithium-ion supercapacitors: Fundamentals and energy applications. 1st ed. Boca Raton: CRC Press/Taylor & Francis; 2018.

[27] Ghossein NE, Sari A, Venet P. Nonlinear Capacitance Evolution of Lithium-Ion Capacitors Based on Frequency- and Time-Domain Measurements. IEEE Transactions on Power Electronics 2018;33:5909-16. https://doi.org/10.1109/TPEL.2017.2745716.

[28] Barcellona S, Piegari L. A lithium-ion capacitor model working on a wide temperature range. Journal of Power Sources 2017;342:241-51. https://doi.org/10.1016/j.jpowsour.2016.12.055.

[29] Soltani M, Beheshti SH. A comprehensive review of lithium ion capacitor: development, modelling, thermal management and applications. Journal of Energy Storage 2020;34:102019. https://doi.org/10.1016/j.est.2020.102019.

[30] Li X, Huang Z, Tian Y, Tian J. Modeling and comparative analysis of a lithium-ion hybrid capacitor under different temperature conditions. International Journal of Energy Research 2020;44:3801-20. https://doi.org/10.1002/er.5168.

[31] Soltani M, De Sutter L, Ronsmans J, van Mierlo J. A high current electro-thermal model for lithium-ion capacitor technology in a wide temperature range. Journal of Energy Storage 2020;31:101624. https://doi.org/10.1016/j.est.2020.101624.

[32] Giakoumis EG. Motorcycles. In: Giakoumis, Evangelos G, editors. Driving and Engine Cycles, Giakoumis EG, Switzerland: Springer International Publishing; 2017, p. 167-191.

[33] Kurnia JC, Sasmito AP. Hydrogen Fuel Cell in Vehicle Propulsion: Performance, Efficiency, and Challenge. In: Sulaiman SA, editor. Energy Efficiency in Mobility Systems, Singapore: Springer;2020, p. 9-26.

[34] Vichard L, Petrone R, Harel F, Ravey A, Venet P, Hissel D. Long term durability test of open-cathode fuel cell system under actual operating conditions. Energy Conversion and Management 2020;212:112813. https://doi.org/10.1016/j.enconman.2020.112813.

[35] Song K, Chen H, Wen P, Zhang T, Zhang B, Zhang T. A comprehensive evaluation framework to evaluate energy management strategies of fuel cell electric vehicles. Electrochimica Acta 2018;292:960-73. https://doi.org/10.1016/j.electacta.2018.09.166.

[36] Vichard L, Harel F, Ravey A, Venet P, Hissel D. Degradation prediction of PEM fuel cell based on artificial intelligence. International Journal of Hydrogen Energy 2020;45:14953-63. https://doi.org/10.1016/j.ijhydene.2020.03.209.

[37] Soltani M, Ronsmans J, Van Mierlo J. Cycle life and calendar life model for lithium-ion capacitor technology in a wide temperature range. Journal of Energy Storage 2020;31:101659. https://doi.org/10.1016/j.est.2020.101659.

[38] Zhang T, Wang P, Chen H, Pei P. A review of automotive proton exchange membrane fuel cell degradation under start-stop operating condition. Applied Energy 2018;223:249-262. https://doi.org/10.1016/j.apenergy.2018.04.049.